Morphology and Interactions of Polymer Brush-Coated Spheres in a Polymer Matrix

JIAJING XU, FENG QIU, HONGDONG ZHANG, YULIANG YANG

Department of Macromolecular Science, The Key Laboratory of Molecular Engineering of Polymers, Ministry of Education of China, Fudan University, Shanghai 200433, People's Republic of China

Received 2 December 2005; revised 18 May 2006; accepted 22 May 2006
DOI: 10.1002/polb.20884
Published online in Wiley InterScience (www.interscience.wiley.com).

ABSTRACT: Using a real space implementation of the self-consistent field theory, we calculated the morphology and interactions of spherical nanoparticles with radius R_p that are grafted by polymer chains of N monomers immersed in a chemically identical polymer melt of polymerization index P. The calculation shows that, for big particles ($R_p \gg N^{1/2}a$, with a the segment size), the interactions and density profiles of the grafted layers are that of brushes at flat interface; While for small particles ($R_p \ll N^{1/2}a$), the interactions and density profiles are characteristic of star polymers. In the case of intermediate grafted chain lengths, that is, $R_p \sim N^{1/2}a$, we found that the grafting density of the polymers and the radius of the spherical nanoparticles are both important in determining the structure and interactions of the grafted layers. Our findings suggest possible ways to tailor the structure and interactions of the nanoparticles to benefit the fabrication of polymeric nanocomposites. ©2006 Wiley Periodicals, Inc. J Polym Sci Part B: Polym Phys 44: 2811–2820, 2006

Keywords: interaction; polymer brushes; polymer matrix; SCFT; sphere

INTRODUCTION

It is of great academic interest and industrial application to graft polymer chains onto surfaces of nanoparticles or colloids. The grafted polymer chains, usually called polymer brushes, can produce interfaces with desired properties and thus modulate interactions between particles, by tailoring the molecular weight and the chemical species of polymer chains.[1–4] Therefore, polymer brushes have been extensively applied to stabilize colloidal dispersions and produce polymeric nanocomposite materials.

The basic properties of polymer brushes have been intensively studied since the pioneering work of Alexander[5] and de Gennes.[6] For a polymer brush immersed in a melt, the equilibrium brush profiles are determined by the competition between the osmotic pressure, which tends to swell the brush, and the elasticity of the grafted chains, which tends to diminish the brush extension. Therefore, the equilibrium brush profiles mainly depend on the following parameters: the molecular weight of the grafted chains, N, and that of the melt chains, P, the curvature of the grafting surface, i.e., the radius of spherical particle, R_p, as well as the grafting density, σ, (which is defined as the average number of grafted chains per surface area of the substrate.)[7]

The most investigated system is the infinite planar brushes (with zero curvature). Shull studied the interaction between two planes in a blend of an adsorbing polymer with one adsorbing end and a nonadsorbing polymer of the same chemical type using the self-consistent field theory (SCFT).[8] When the molecular weight of the adsorbing polymers N is greater than or equal to that of the nonadsorbing polymers P ($N \geq P$), the interaction between the two planes is purely repulsive; other-

Correspondence to: F. Qiu (E-mail: fengqiu@fudan.edu.cn) or Y. Yang (E-mail: ylyang@srcap.stc.sh.cn)

Journal of Polymer Science: Part B: Polymer Physics, Vol. 44, 2811–2820 (2006)
©2006 Wiley Periodicals, Inc.

wise ($N < P$), there is an attractive interaction due to the interpenetration of the opposing brushes, and the concomitant expelling of the free chains from the brush layers. Ferreira et al. systematically explored the parameter space of the chemically-grafted planar polymer brushes in a melt.[9] Their results show that because of subtle entropic effects, the free chains in the melts are expelled from the grafted layers, even if they are chemically identical to the grafted chains, and the interactions between the brushes can be purely repulsive or repulsive at short distances and attractive at longer distances. The region where attraction exists satisfies $\sigma N^{1/2} > (N/P)^2$. However, in a similar system, Matsen found that there is always an attractive interaction between the two brushes immersed in melts, which is ascribed to the positive interfacial tension between the brushes and the melt chains.[10]

Recent experimental progress in polymer brush coated nanoparticles or nanorods raises the question of the curvature effects on the brush interactions. The existing relevant theoretical studies only considered spherical brushes in small molecule solvents. Lin and Gast found that the interaction of spherical brushes in a molecular solvent is purely repulsive over a wide range of the radius of curvature of the spherical brushes, the length of the grafted polymers, and the grafting density.[11] Wijmans et al. predicted that the interactions between spherical brushes are far less repulsive than that would be expected from the interactions between two equivalent flat surfaces. This is explained by the greater freedom of the grafted chains to move laterally out of the widening gap between the spherical particles when compared with the chains between flat surfaces.[12] However, Roan and Kawakatsu developed a new SCFT method to take into account the redistribution of the segment density along the direction parallel to the particle surface when the two interacting spherical brushes approach each other, and predicted attractive interaction potentials between spherical brushes even in a molecular solvent.[13]

There are rare investigations on systems of spherical brushes immersed in polymer matrix with brush core size 10–100 nm and thickness of about the same size, which is the most relevant to practical polymeric nanocomposites.[14] For slightly curved spherical brushes dispersed in a melt of long polymer chains, Hasegawa et al. found that the interaction potential of the brushes shows an attractive minimum, which becomes very shallow at an intermediate grafting density; while at lower or higher grafting densities, the attractive interactions become stronger, and therefore, the particles form clusters within the polymer matrix.[15] We studied the interaction between brush-coated clay sheets in a polymer matrix.[16] Our calculation showed that the lateral dimension of the clay sheets is a new relevant length scale in determining the structure and interactions of the grafted layers.

In most of the previously studied systems, the radius of curvature of the grafted surface is much larger than that of the polymer chain, and in this case, the distribution of the grafting ends on the grafted surface is trivial, and no extra effort is needed to ensure the homogeneity of the grafting points. However, when the radius of curvature of the grafted surface is around the size of polymer chain, the lateral homogeneity of the grafting ends cannot be satisfied automatically without additional treatments. Roan and Kawakatsu adopted the special initial condition for the grafting ends to achieve the constraint.[13] In this article, we introduce a Lagrangian multiplier method to constrain the grafting point distribution in SCFT and use it to study the structure and interaction between spherical polymer brushes in the melts of the same chemical type.

The formalism of the model is briefly described (*see Model section*) with special focus on the Lagrangian multiplier method to constrain the grafting point distribution. The results of the calculation are presented and discussed in detail (*see Results and Discussions section*). Finally, the main conclusions are summarized.

MODEL

Self-Consistent Field Theory

The system we considered is composed of two identical polymer grafted spherical particles immersed in a polymer matrix, as illustrated in Figure 1. The system is sufficiently large so that the influence of the brushes ceases to exist at the boundaries and the melt chains attain their bulk properties. The bulk is characterized by a constant mean density of monomers $\phi_b = 1$. The radius of the particles is R_p, and the closest distance between them is D. Each of the particles is grafted with $n_\alpha/2$ polymer chains of polymerization index N, and the polymer matrix has n_β free chains of polymerization index P. The monomers of the grafted chains and the free chains are assumed to

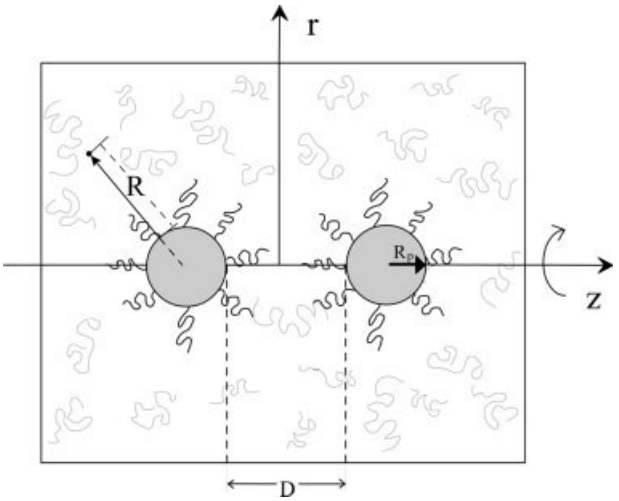

Figure 1. Schematic diagram of the geometry of two brush-coated spherical particles in a polymer melt. The system has a rotational symmetry about the *z*-axis, thus only a cross section in the *rz*-plane is drawn. The two particles are represented by two circles and the grafted chains are drawn in black and the melt chains are in gray. Note that R_p is the sphere radius, and D is the closest distance between the two spheres, R is the distance away from the particle surface.

be chemically identical, flexible with a statistical length a (Kuhn length), and incompressible with a volume ρ_0^{-1}. The volume occupied by the polymers is $V = (n_\alpha N + n_\beta P)\rho_0^{-1}$.

Each of the grafted polymer chains and the free polymer chains are modeled as Gaussian chain that is described by a continuous curve $R_\alpha(s)$ or $R_\beta(s)$ representing all possible configurations of the macromolecules. The variable s increases continuously along the length of the chain. For grafted chain, $s = 0$ at the particle surfaces and $s = N$ at its free extremity, the grafted extremity is named as "grafting end" in this article. In the case of free polymer chains, the two extremities are identical, and $s = 0$ at one of the extremity and $s = P$ at the other extremity. For Gaussian chains, the possibility density functional for a given configuration is of the Wiener form:

$$P[R_\alpha(\cdot)] \propto \exp\left[-\frac{3}{2a^2}\int_0^N ds\left(\frac{\partial R_\alpha(s)}{\partial s}\right)^2\right] \quad (1)$$

and $P[R_\beta(\cdot)]$ can be given by a similar expression with N replaced by P. Therefore, the monomer density operators $(\hat{\phi}_\alpha, \hat{\phi}_\beta)$ and the grafting ends density operator $(\hat{\phi}_{s=0})$ can be defined as

$$\hat{\phi}_\alpha(\mathbf{r}) = \rho_0^{-1}\sum_{\alpha=1}^{\pi_\alpha}\int_0^N ds\delta[\mathbf{r} - R_\alpha(s)] \quad (2a)$$

$$\hat{\phi}_\beta(\mathbf{r}) = \rho_0^{-1}\sum_{\beta=1}^{\pi_\beta}\int_0^p ds\delta[\mathbf{r} - R_\beta(s)] \quad (2b)$$

$$\hat{\phi}_{s.0}(\mathbf{r}) = \rho_0^{-1}\sum_{\alpha=1}^{\pi_\alpha}\delta[\mathbf{r} - R_\alpha(s=0)] \quad (2c)$$

The surfaces of the spherical particles where the polymer chains are tethered on are denoted as $\mathbf{r}_c$. The distribution of the grafting ends on the particle surface is specified by the local grafting density $\sigma(\mathbf{r}_c)$, which means the area fraction of surface occupied by the grafting end at point $\mathbf{r}_c$. We can also define a volume fraction grafting end distribution and have the relationship $\sigma_v(\mathbf{r}) = k\sigma(\mathbf{r}_c)\delta(\mathbf{r}-\mathbf{r}_c)$, where k is a trivial constant set to 1 in this article. Therefore, $n_\alpha = \int d\mathbf{r}\sigma_v(\mathbf{r}) = \int d\mathbf{r}_c\sigma(\mathbf{r}_c)$.

The canonical partition function of this system can be written as:

$$Z = \prod_{\alpha=1}^{\pi_\alpha}\int DR_\alpha(\cdot)P[R_\alpha(\cdot)] \times \prod_{\beta=1}^{\pi_\beta}\int DR_\beta(\cdot)P[R_\beta(\cdot)] \times \prod\nolimits_{\mathbf{r}}\delta(1-\hat{\phi}_\alpha-\hat{\phi}_\beta) \times \prod\nolimits_{\mathbf{r}_c}\delta(\sigma_v - \hat{\phi}_{s=0}) \quad (3)$$

where $D\mathrm{R}_\alpha(\cdot)$ and $D\mathrm{R}_\beta(\cdot)$ denote the functional integration over all possible configurations of the chains, and the first δ function selects the configurations satisfying the local incompressibility constraint of the melts, and the second δ function ensures the distribution of grafting ends satisfies certain constraints. We had just neglected all the interactions between the particles and the interactions between the chains and the particles. Because of the fact that the grafted polymer chains and the free chains are chemically identical, there is not an explicit expression for the interaction potential between the grafted chains and the free polymer chains.

Using the Hubbard-Stratonovich transformation, the canonical partition function can be rewritten as

$$Z = \int D\phi_\alpha D\phi_\beta Dw_\alpha Dw_\beta D\xi \exp\{-\beta\Phi\} \quad (4)$$

with the functional

$$\beta\Phi = -\rho_0\int d\mathbf{r}\{w_\alpha(\mathbf{r})\phi_\alpha(\mathbf{r}) + w_\beta(\mathbf{r})\phi_\beta(\mathbf{r}) + \xi(\mathbf{r})[1-\phi_\alpha(\mathbf{r})-\phi_\beta(\mathbf{r})] + \pi(\mathbf{r})\sigma_v(\mathbf{r})\} - n_\alpha\ln(Q_\alpha/V) - n_\beta\ln(Q_\beta/V) \quad (5)$$

where $\beta = 1/k_BT$ with the Boltzmann constant k_B and the temperature T. $\phi_\alpha(\mathbf{r})$, $\phi_\beta(\mathbf{r})$, and $\phi_{s=0}(\mathbf{r})$ are the local volume fractions of the grafted and free chains, and the density of the grafting ends, respectively. $w_\alpha(\mathbf{r})$ and $w_\beta(\mathbf{r})$ are the corresponding self-consistent fields, and the pressure field $\xi(\mathbf{r})$ ensures the local incompressibility of the system, and the Lagrangian multiplier field $\pi(\mathbf{r})$ constrains the distribution of the grafting ends. The single chain partition functions Q_α and Q_β are defined as

$$Q_\alpha = \int D\mathrm{R}_\alpha(\cdot)P[\mathrm{R}_\alpha(\cdot)]\exp\{-\pi[\mathrm{R}_\alpha(s=0)] - \int_0^N ds w_\alpha[\mathrm{R}_\alpha(s)]\} = \int d\mathbf{r} q_\alpha(\mathbf{r},N) \quad (6a)$$

$$Q_\beta = \int D\mathrm{R}_\beta(\cdot)P[\mathrm{R}_\beta(\cdot)]\exp\left\{-\int_0^P ds w_\beta[D\mathrm{R}_\beta(s)]\right\} = \int d\mathbf{r} q_\beta(\mathbf{r},P) \quad (6b)$$

where the canonical statistical weight of the subchain $q(\mathbf{r},s)$ represents the probability of finding segment s at position $\mathbf{r}$.[17] $q(\mathbf{r},s)$ obeys the modified diffusion equations with proper initial condition. For example, for the grafted chains,

$$\frac{\partial q_\alpha(\mathbf{r},s)}{\partial s} = \frac{a^2}{6}\nabla^2 q_\alpha(\mathbf{r},s) - w_\alpha(\mathbf{r})q_\alpha(\mathbf{r},s) \quad (7)$$

with the initial condition for eq 7 is $q_\alpha(\mathbf{r},0) = \exp[-\pi(\mathbf{r})]$. Because the two ends of the grafted chains are distinct, a second end-segment distribution function, $q_\alpha^\dagger(\mathbf{r},s)$, is needed. It satisfies eq 7 with the right-hand side multiplied by -1, and the initial condition, $q_\alpha^\dagger(\mathbf{r},N) = 1$. For the free chains ($\beta$ chains), the two ends are identical, therefore, $q_\beta^\dagger(\mathbf{r},P-s) = q_\beta(\mathbf{r},s)$ and the equation of $q_\beta(\mathbf{r},s)$ is similar to eq 7 with the initial condition, $q_\beta(\mathbf{r},0) = 1$.

It is impossible to complete the functional integral to get the partition function, so we will take the saddle point approximation,

$$\beta F \approx -\ln Z_{\max} = \beta\Phi_{\min}(w_\alpha, w_\beta, \phi_\alpha, \phi_\beta, \xi, \pi) \quad (8)$$

Minimizing the functional in eq 5 with respect to the six variables (w_α,w_β,ϕ_α,ϕ_β,ξ,π), leads to a set of equations:

$$w_\alpha(\mathbf{r}) = \xi(\mathbf{r}) \quad (9a)$$

$$w_\beta(\mathbf{r}) = \xi(\mathbf{r}) \quad (9b)$$

$$\phi_\alpha(\mathbf{r}) = \rho_0^{-1}n_\alpha\frac{\int_0^N ds q_\alpha(\mathbf{r},s)q_\alpha^\dagger(\mathbf{r},s)}{\int d\mathbf{r} q_\alpha(\mathbf{r},N)} \quad (9c)$$

$$\phi_\beta(\mathbf{r}) = \rho_0^{-1}n_\beta\frac{\int_0^P ds q_\beta(\mathbf{r},s)q_\beta(\mathbf{r},P-s)}{\int d\mathbf{r} q_\beta(\mathbf{r},P)} \quad (9d)$$

$$\phi_{s=0}(\mathbf{r}) = \rho_0^{-1}n_\alpha\frac{q_\alpha(\mathbf{r},0)q_\alpha^\dagger(\mathbf{r},0)}{\int d\mathbf{r} q_\alpha(\mathbf{r},N)} \quad (9e)$$

$$1 - \phi_\alpha(\mathbf{r}) - \phi_\beta(\mathbf{r}) = 0 \quad (9f)$$

$$\sigma_v(\mathbf{r}) - \phi_{s=0}(\mathbf{r}) = 0 \quad (9g)$$

eqs 9a–9g can be solved in a self-consistent way to determine the free energy of systems.[16,18,19] In practical calculations, the constraints $\phi_\alpha(\mathbf{r}) + \phi_\beta(\mathbf{r}) = 1$ and $\phi_{s=0}(\mathbf{r}) = \sigma_v(\mathbf{r})$ are realized by choosing the pressure field ξ and Lagrange multiplier field π according to

$$\xi(\mathbf{r}) = \xi_0[1 - \phi_\alpha(\mathbf{r}) - \phi_\beta(\mathbf{r})] \quad (10)$$

$$\pi(\mathbf{r}) = \pi_0[\phi_{s=0}(\mathbf{r}) - \sigma_v(\mathbf{r})] \quad (11)$$

where ξ_0 and π_0 are trivial constants, and the resulting density profiles and energies are independent of their particular values.[9]

The interaction free energy for the two brushes separated at a distance D, $U(D)$, is defined as

$$U(D) = \beta[F(D) - F(\infty)] \quad (12)$$

where the reference state is taken to be the state where the two spherical brushes are separated far enough so that the monomer density distributions are not altered even when they are separated further.

Numerical Method

Since the system has rotational symmetry about the axis that passes through the two centers of the spheres, it is convenient to perform the calculations in a cylindrical coordinates, as shown in Figure 1. Because all the variables have no azimuthal dependence, we solve the SCFT equations in a 2D coordinate (r, z). The modified diffusion equations can be written as

$$\frac{\partial q(r,z,s)}{\partial s} = \frac{a^2}{6}\left[\frac{\partial^2 q(r,z,s)}{\partial z^2} + \frac{1}{r}\frac{\partial q(r,z,s)}{\partial r} + \frac{\partial^2 q(r,z,s)}{\partial r^2}\right] - w(r,z)q(r,z,s) \quad (13)$$

where q can be q_α, $q_\alpha^\dagger$, q_β, and w can be w_α, w_β. We adopt the hard wall boundary condition on the

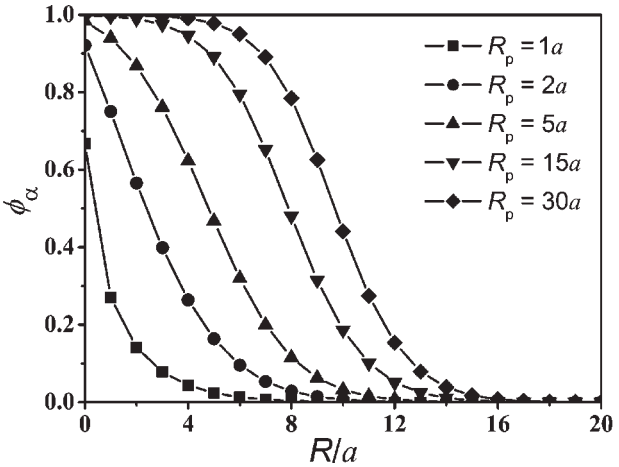

Figure 2. The density profiles for isolated spherical brushes at various particle radii with $N = P = 50$ and $\sigma = 0.30$.

sphere surface, that is, $q(\mathbf{r} \in \Omega,s) = 0$, where Ω is the space occupied by the particles, and the no-slope boundary condition on the outer boundary of the system, both in r and z directions: $\partial q\ (r = 0,z,s)/\partial r = 0$; $\partial q(r = L_r,z,s)/\partial r = 0$; $\partial q(r,z = 0,s)/\partial z = 0$; $\partial q(r,z = L_z,s)/\partial z = 0$. Correspondingly, taking the single chain partition function Q_α as an example, the integration of any quantities in polar coordinate is evaluated as

$$Q_\alpha = \int q_\alpha(r,z,s)q_\alpha^\dagger(r,z,s)2\pi r dr dz \qquad (14)$$

In fact, to fully exploit the symmetry of the system, we chose only a quarter of the whole system to carry out the calculations with the above mentioned boundary conditions. The size of the system is chosen such that $L_r \gg R_p + N^{1/2}a$ and $L_z \gg 2(R_p + N^{1/2}a)$ to avoid finite size effect.

The SCFT equations are solved using a numerical real space iteration method. The algorithm starts with initial fields. Using a Crank-Nicholson scheme and an alternating-direction implicit (ADI) method,[20] the diffusion equations are then integrated to obtain $q_\alpha(q_\beta)$ and $q_\alpha^\dagger$, for $0 \le s \le N(P)$. The right-hand side of eqs 9c and 9d are evaluated to obtain new expressions for the volume fractions of the different species. The final step is updating the potential fields using eqs 9a, 9b, 10, and 11 by means of a linear mix of new and old solutions. These steps are repeated until the incompressibility of the system satisfies $|1 - \phi_\alpha(\mathbf{r}) - \phi_\beta(\mathbf{r})| \le 10^{-7}$, and the free energy change at each iteration is reduced to 10^{-6}. For details of the algorithm, the readers are referred to Ref. 16.

RESULTS AND DISCUSSIONS

In this section, the structure and the density profile of the grafting chain are described and then the interaction between the brushes is discussed in connection with the morphology. To emphasis the effects of variations of grafting density and particle radius, we set $N = P = 50$ and assume the homogeneous grafting density for all the data and results presented if without additional specification.

Morphology

First, we will discuss how the particle radius and grafting density affect the structure of an independent brush. Figure 2 shows the monomer density profiles for $\sigma = 0.30$ with different radii of the sphere, R_p. These profiles demonstrate an obvious influence of the sphere radii on the structure of the grafted chain layer. When $R_p \ge N^{1/2}a$, the monomer density profiles are the parabolic, which are characteristic of polymer brushes at a flat interface; when $R_p \le N^{1/2}a$, the density profiles are the power law decay, which is typical of a star polymer. A similar behavior has also been observed in a spherical brush in solutions,[11] in which by decreasing the core curvature, the structure of grafted layer was considered to change from those in star polymers to planar brushes. In the present calculations, however, without any further approximation, with the continuously changing radius of the spheres, the similar structure variations are predicted for brushes in melts.

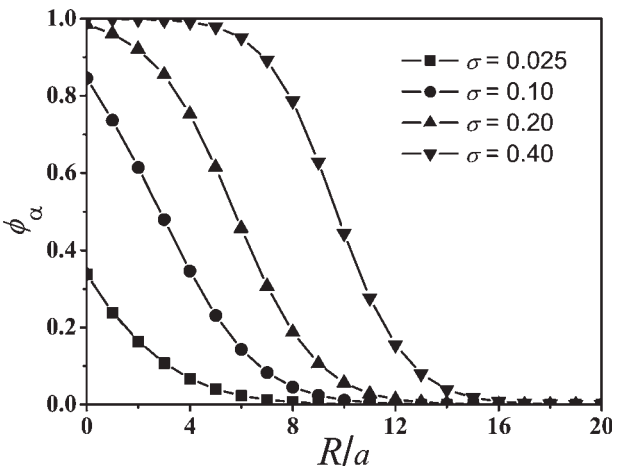

Figure 3. The density profiles for isolated spherical brushes at different grafting densities with $R_p = 15a$ and $N = P = 50$.

The grafting density of the polymer chains also alters the structure of the spherical brushes. As an example, we illustrate in Figure 3 the monomer density profiles of the brush at different grafting densities with $R_p = 15a$. By increasing the grafting density, the change of the density profiles, i.e., from the parabolic to the power law decay, is observed. More specifically, when the grafting density is low, $\sigma N^{1/2} \ll 1$, i.e., $\sigma \ll 0.14$ the free melt polymer chains penetrate the brush ("wet brush"); when the grafting density is high enough, $\sigma N^{1/2} \gg 1$, i.e., $\sigma \gg 0.14$, the melt chains are expelled from the brush ("dry brush"). The interface between the brush and the melt, however, is not sharp; the melt penetrates over a distance inside the brush. This phenomenon arises as a balance between two effects. On the one hand, the penetration of free chains into the brush is entropically favorable; on the other hand, the melt penetration implies an extra stretching of the chains in the outer fringe of the brush and a subsequent cost in the elastic free energy.

We have discussed the structure of an isolated brush, which is true for brushes at great separation $D \gg Na$. When two brushes are close to each other, apparently, the interaction between the two spherical brushes will alter their structure. In Figure 4, the distributions of the monomer density for brushes at different distances D with $R_p = 15a$ are illustrated as an example.

For convenience, the part of each sphere surface facing each other will be referred to as front surface and the rest part as rear surface, and correspondingly, the brushes grafted on the front and rear surfaces are named the front and rear brushes, respectively. From Figure 4, we know for the value of $\sigma(= 0.50)$, the brushes are well in the "dry" brush regime (where $\sigma N^{1/2} \geqslant 1$). When the two spheres are far away from each other, no obvious structure change is observed. The melt polymer chains occupy the space between the separated front brushes, and one finds that the monomer density of the grafted chains is almost zero in this area. As the distance between the spheres decreases and reaches some value where the fringes of the two front brushes start to touch each other, the melt chains being expelling out from this area. If the distance of the two spheres is further decreased, the two grafted layers start to compress each other, and one can see that almost all the free chains are expelled out. As for the density profile of the rear brushes, it remains almost unchanged as the two spheres approach each other.

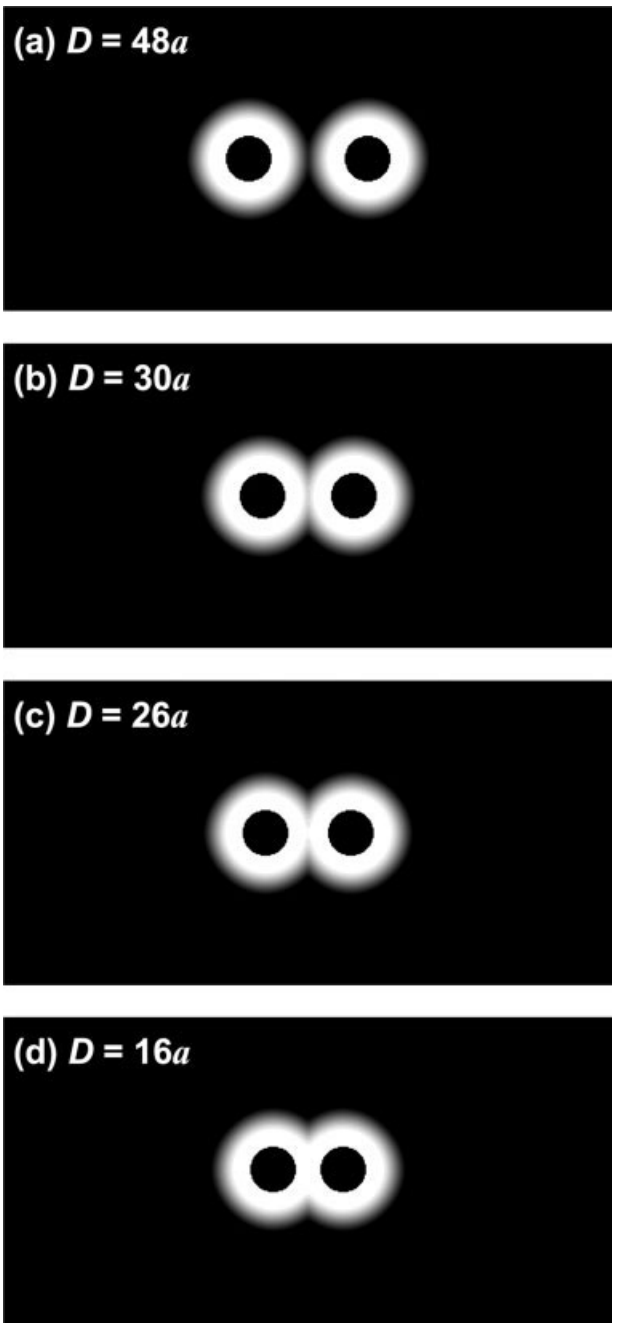

Figure 4. Distribution of segment density of two approaching spherical polymer brushes with $R_p = 15a$, $N = P = 50$, and $\sigma = 0.50$ and different distances of the two spheres, D. The segment density in the white region is higher than that in the dark region and the dark circle in the center of the white region represents the spherical core of the particles. From top to bottom, the closest distances between the spherical brushes are $48a$, $30a$, $26a$, and $16a$, respectively.

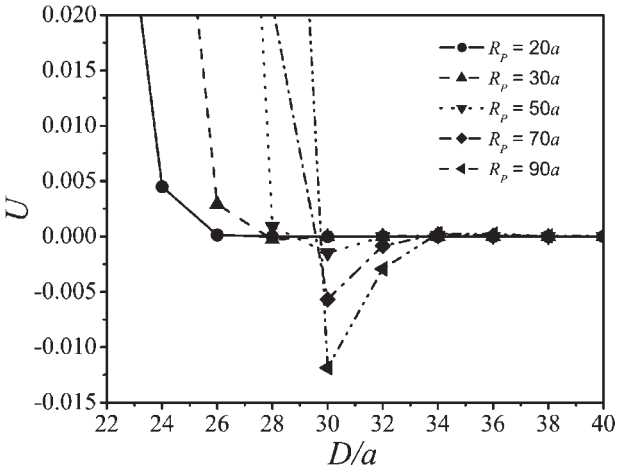

Figure 5. The interaction free energy of the two brushes as a function of the distance between them with various particle radii at $N = P = 50$ and $\sigma = 0.30$.

Interaction Between Spherical Brushes

In Figure 5, we present the interaction free energy $U(D)$ of the two spherical brushes in a melt as a function of the distance D between them, for different values of the sphere radius R_p. The five curves plotted in Figure 5 correspond to the five values of the sphere radius $R_p = 20a$ (circle), $R_p = 30a$ (triangle up), $R_p = 50a$ (triangle down), $R_p = 70a$ (diamond), and $R_p = 90a$ (triangle left).

As we expected, at small brush separations there is a repulsive part in the interaction free energy for all the five cases because of the excluded volume effect between the grafted polymers. While at large brush separations, there is no interaction between the brushes. Surprisingly, at intermediate distances (roughly at the contact distance of the fringes of the two brushes), however, the interactions are attractive for relatively large spheres. More specifically, it is observed that for $R_p \gg N^{1/2}a$, at intermediate distances the interactions are attractive; however, for $R_p \sim N^{1/2}a$, there is no observable attraction. In fact, for $R_p \ll N^{1/2}a$, the structure of the grafted layers appears like that of star polymers, and only repulsion is possible. Therefore, our SCFT calculations show that the radius of the spheres is indeed a new relevant length scale in the problem, which we considered here, and decreasing the radius of the spheres can cause a substantial change in the interacting force between the spheres.

Increasing the grafting density has the similar effect as to increasing particle radius, as is presented in Figure 6. The four curves plotted in Figure 6 correspond to the four values of the grafting density for $R_p = 15a$ at $\sigma = 0.2$(circle), $\sigma = 0.4$(triangle up), $\sigma = 0.5$(triangle down), and $\sigma = 0.6$(diamond). There is an attractive part in the interaction free energy if σ is larger than a certain value. Therefore, we conclude that the appearing of the attractive interaction can be caused by increasing either the grafting density or the sphere radius.

To identify the origin of the attractive interaction, the total free energy of the system is divided into two parts: the contribution from the grafted chains F_α, and that from the free chains F_β, respectively:

$$\frac{F_\alpha}{k_B T} = -\rho_0 \int d\mathbf{r} w_\alpha(\mathbf{r}) \phi_\alpha(\mathbf{r}) - n_\alpha \ln\left\{Q_\alpha/V\right\} \quad (15a)$$

$$\frac{F_\beta}{k_B T} = -\rho_0 \int d\mathbf{r} w_\beta(\mathbf{r}) \phi_\beta(\mathbf{r}) - n_\beta \ln\left\{Q_\beta/V\right\} \quad (15b)$$

We take the case with $R_p = 15a$ and $\sigma = 0.5$ as an example, which is shown in Figure 7. Several important features are observed: (1) It is clear that in most of the interaction range presented, since the grafted chains are not extremely deformed, the contribution from the melt chains F_β dominates the total free energy F ($= F_\alpha + F_\beta$). (2) At the intermediate distance between the spherical brushes, the free energy of the free chains shows a minimum. The reason is that, before the fringes of the two front layers compress each other too much, moving closer to each other leads to a larger space for the free chains, which is entropi-

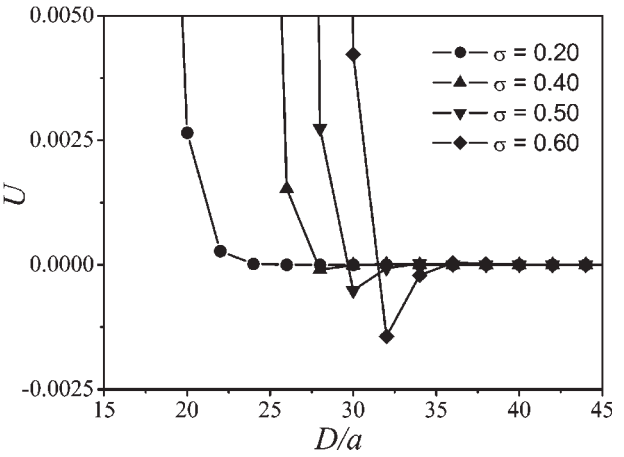

Figure 6. The interaction free energy of the two approaching brushes as a function of the distance between them with different grafting densities at $N = P = 50$ and $R_p = 15a$.

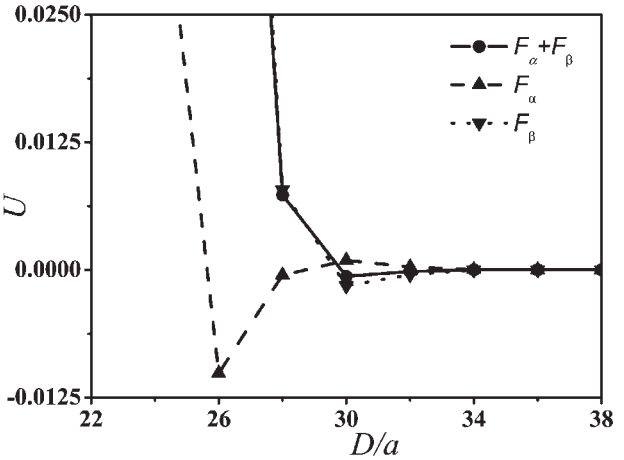

Figure 7. The interaction free energy and the two contributions from the grafted and free chains with $R_p = 15a, N = P = 50$ and $\sigma = 0.50$.

cally favorable. As the two front layers are further compressed, however, the free chains immersed in the layers are stretched,[21] which is entropically unfavorable and thus leads to an increase of the free energy. (3) For the grafted chains, there is also a minimum at the intermediate distance of the two brushes. We ascribe the lowering of the free energy to the redistribution of the grafted chains (not the grafted ends) because of the spherical geometry, which obtains entropy; while further decreasing the distance between the two spheres, the grafted layers are too much compressed, resulting in great lose of entropy and hence increasing the free energy. We note that the redistribution of polymer segments to acquire additional configurational entropy was also observed in spherical polymer brushes in small molecular solvents.[13] (4) The interesting fact is that the distance at which the minimum of the free energy of the grafted chains appears is shorter than that of the free chains. As the minimum of F_α is reached, the value of F_β is already very high, which explains why only one minimum is observed in the total free energy. Finally, we would like to note that when the two spheres are moved very close (which is not shown in Figure 7), the two front layers are extremely compressed, thus the free chains are all expelled from the front layers, as expected, the free energy contribution from the grafted chains F_α dominates the total free energy.

Hence, we think the attractive potential arises mainly from the free chains in the melts rather than the grafted chains, which agrees with the opinion of Hasegawa et al.[15] In their work, the particles were so big that the grafting surfaces could be taken as planar surface. However, our SCFT calculations show that the radius of the particles is indeed a new relevant length scale in the problem, which we consider here, and decreasing the radius of the spheres can cause a substantial change in the interacting force between the particles. In addition, their theoretical works were carried out in a one-dimensional space, and thus the redistribution of grafted chains to acquire additional entropy could not be taken into account.

Figure 8 presents the distances at which the minimum of the interaction free energy is attained for various values of σ and R_p. Since the effective attraction between the brushes results from the replacement of the two unfavorable brush-melt interfaces by a single brush-brush interface, the distance at which the attraction attains its maximum value (denoted by D_{min}) is roughly the sum of the two equilibrium brush heights (marked by h), that is, $D_{min} \propto h \propto aN\sigma$. Indeed, it is seen from Figure 8 that all the curves are straight lines. Furthermore, the slopes of the lines appear to be dependent on the value of $R_p/N^{1/2}a$. For high enough values of $R_p/N^{1/2}a$, the radius is not relevant in determining the peak position. However, decreasing the value of $R_p/N^{1/2}a$ decreases the slope of the lines, which means that in the intermediate regime ($R_p \sim N^{1/2}a$) the radius of the spheres is relevant and the peak position is affected by this length scale.

We note that in Ref. 15, a similar system was investigated by a mean field calculation and an optimum grafting density giving the least depth of the attraction was found. In fact, the optimum

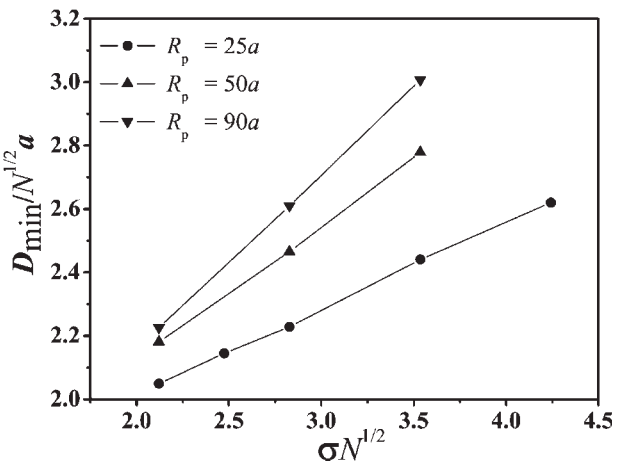

Figure 8. The location of the minimum of the interaction free energy (D_{min}) as a function of the grafting density σ for different particle radii R_p.

grafting density in Ref. 15 comes from the balance between two different interactions: one is the van der Waals interaction between the spherical particles, which is always attractive (especially at shorter distances); the other is the interaction caused by the grafting and free (matrix) polymers, which is repulsive at short distance and attractive at longer distance, depending on the grafting density, the particle size, and the free chain length. However, to simplify the problem and emphasize the effect of grafting, the van der Waals interaction is not considered in the present article, thus there is no optimum grafting density found. Considering the van der Waals interaction is trivial, and we expect that there must exist an optimum grafting density that gives the least depth of the attraction, since the interaction caused only by polymer grafting (see Figure 6) behaves similarly to that calculated in Ref. 15.

Migration of Grafting Ends

In the above calculations, we ensure the fixing of the grafting ends by iterating the potential $\pi(\mathbf{r})$. Such constraint is necessary to consider spherical brushes with fixed grafting density. On the other hand, if we remove the constraint, that is, setting $\pi(\mathbf{r}) = 0$, we can demonstrate how the grafted ends migrate with different separation between the brushes, which reflects the interaction between the grafted polymer chains.

To show the redistribution of the grafting ends more clearly, we introduced a new variable $\gamma(\mathbf{r}_c)$ to measure the degree of redistribution, which is defined as:

$$\gamma(\mathbf{r}_c) \equiv \frac{\phi_{s=0}(\mathbf{r}_c)|_D}{\phi_{s=0}(\mathbf{r}_c)|_{D=\infty}} \tag{16}$$

It is the ratio the grafting density at the same position on the surface of spherical particle when the separation between the two particles is D to that when the separation is far away enough. It reflects the redistribution of the grafting ends when two brushes approach. If its value is closer to 1, it means that less redistribution occurs.

In Figure 9, when the approaching spherical brushes with $R_p = 15a$ at different separation, the migration of the grafting ends is illustrated. At the separation ($D = 30a$) where the interaction free energy minimum occurs, we can find that the redistribution of the grafting ends is unnoticeable. However, when the spherical brushes is approaching closer (in (b) $D = 22a$, and in (c) $D = 20a$), the

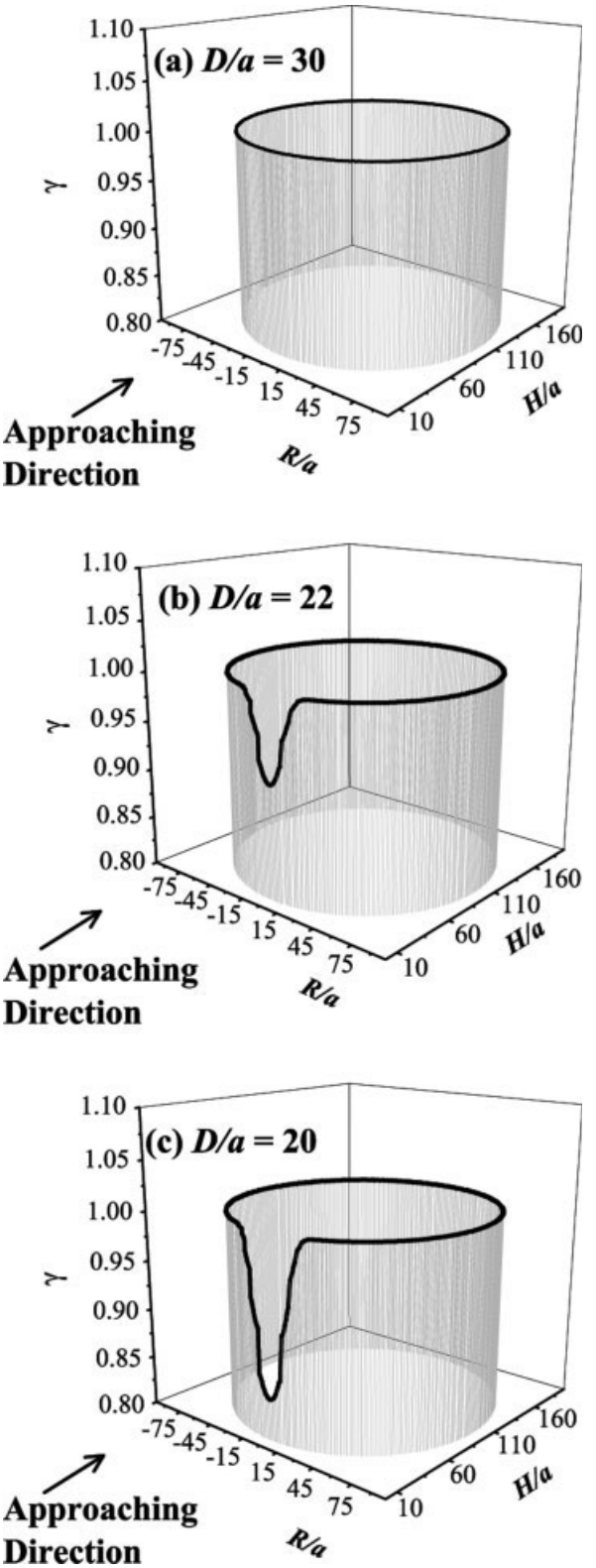

Figure 9. The migration of the grafting ends reflected using $\gamma(\mathbf{r}_c)$, when two spherical brushes approaching each other with the particle radius $R_p = 90a$, grafting density $\sigma(\mathbf{r}_c) = 0.30$. (a) $D = 30a$; (b) $D = 22a$; (c) $D = 20a$.

redistribution of the grafting ends become more greater, the grafting ends migrate away from the front surfaces laterally, eventually to the rear surfaces.

CONCLUSIONS

The morphology and interaction of brush-coated spheres immersed in a polymer melt have been systematically analyzed by the real space SCFT algorithm, with special focus on the grafting density σ and the size of the spheres R_p. Because of the subtle entropy effect, the interactions between the two spherical layers show an attractive part by varying either the grafting density σ or the radius of the spheres R_p at the fixed polymerization indexes of the grafting chains N and the matrix (free) chains P. The free chain exclusion and the grafted chain redistribution are responsible for the appearance of the attractive minimum in the interaction energy of two brushes immersed in a chemically identical polymer melt.

It is straightforward to extend the present model to other complicated yet still realistic situations, for example, if the grafted chains and the matrix chains are chemically different, either incompatible or attractive, the structure and interaction of the grafted layers are greatly influenced. In conclusion, the present SCFT model bridges the gap between the existing models for brushes grafted on flat interface and stars of polymer chains tethered to a central microscopic core. Such a model would be useful to investigate the structure and phase diagrams of the experimental systems such as self-assembly of grafted nanoparticles immersed in polymer matrix, colloidal stabilization in a polymer solution, and wetting of protected surfaces by polymeric materials. The findings may have various implications for creating novel polymeric nanocomposites.

We gratefully acknowledge financial support from the National Basic Research Program of China (grant no. 2005CB623800) and the NSF of China (grant nos. 20104002, 20234010, 20374016, and 20221402). F. Qiu acknowledges Ministry of Education of China (FANEDD 200225) and STCSM (grant no. 02QE14010).

REFERENCES AND NOTES

1. Giannelis, E. P.; Krishnamoorti, R. K.; Manias, E. Adv Polym Sci 1999, 138, 107.
2. Yano, K.; Uzuki, A.; Okada, A.; Kamigaito, O. J Polym Sci Part A: Polym Chem 1993, 31, 2493.
3. Manias, E.; Touny, A.; Wu, L.; Strawhecker, K.; Chung, T. C. Chem Mater 2001, 13, 3516.
4. Vaia, R. A.; Vasudevan, S.; Krawiec, W.; Scanlon, L. G.; Giannelis, E. P. Adv Mater 1995, 7, 154.
5. Alexander, S. J Phys (France) 1977, 38, 983.
6. de Gennes, P. G. Macromolecules 1980, 13, 1069.
7. Aubouy, M.; Fredrickson, G. H.; Pincus, P.; Raphaeel, E. Macromolecules 1995, 28, 2979.
8. Shull, K. R. J Chem Phys 1991, 94, 5723.
9. Ferreira, P. G.; Ajdari, A.; Leibler, L. Macromolecules 1998, 31, 3994.
10. Matsen, M. W.; Gardiner, J. M. J Chem Phys 2001, 115, 2794.
11. Lin, E. K.; Gast, A. P. Macromolecules 1996, 29, 390.
12. Wijmans, C. M.; Leermakers, F. A. M.; Fleer, G. J. Langmuir 1994, 10, 4514.
13. Roan, J. R.; Kawakatsu, T. J Chem Phys 2002, 116, 7295.
14. Yezek, L.; Schärtl, W.; Chen, Y.; Gohr, K.; Schmidt, M. Macromolecules 2003, 36, 4226.
15. Hasegawa, R.; Aoki, Y.; Doi, M. Macromolecules 1996, 29, 6656.
16. Wang, R.; Qiu, F.; Zhang, H. D.; Yang, Y. L. J Chem Phys 2003, 118, 9447.
17. Doi, M.; Edwards, S. F. The Theory of Polymer Dynamics; Oxford University Press: Oxford, England, 1986.
18. Drolet, F.; Fredrickson, G. H. Phys Rev Lett 1999, 83, 4317.
19. Drolet, F.; Fredrickson, G. H. Macromolecules 2001, 34, 5317.
20. Press, W. H.; Flannery, B. P.; Teukolsky, S. A.; Vetterling, W. T. Numerical Recipes; Cambridge University Press: Cambridge, England, 1989.
21. Martin, J. I.; Wang, Z. G. J Phys Chem 1995, 99, 2833.